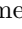
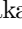
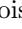






















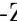









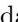



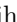







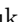



Search for lepton flavor-violating decay modes $B^0 \rightarrow K_S^0 \tau^\pm \ell^\mp$ ($\ell = \mu, e$) with hadronic B -tagging at Belle and Belle II

- I. Adachi , K. Adamczyk , L. Aggarwal , H. Ahmed , H. Aihara , N. Akopov , M. Alhakami , A. Aloisio , N. Althubiti , N. Anh Ky , D. M. Asner , H. Atmacan , V. Aushev , M. Aversano , R. Ayad , V. Babu , H. Bae , N. K. Baghel , S. Bahinipati , P. Bambade , Sw. Banerjee , S. Bansal , M. Barrett , M. Bartl , J. Baudot , A. Baur , A. Beaubien , F. Becherer , J. Becker , J. V. Bennett , F. U. Bernlochner , V. Bertacchi , M. Bertemes , E. Bertholet , M. Bessner , S. Bettarini , V. Bhardwaj , B. Bhuyan , F. Bianchi , D. Biswas , A. Bobrov , D. Bodrov , A. Bolz , A. Boschetti , A. Bozek , M. Bračko , P. Branchini , R. A. Briere , T. E. Browder , A. Budano , S. Bussino , Q. Campagna , M. Campajola , L. Cao , G. Casarosa , C. Cecchi , J. Cerasoli , M.-C. Chang , P. Chang , R. Cheaib , P. Cheema , B. G. Cheon , K. Chilikin , K. Chirapatpimol , H.-E. Cho , K. Cho , S.-J. Cho , S.-K. Choi , S. Choudhury , J. Cochran , L. Corona , J. X. Cui , E. De La Cruz-Burelo , S. A. De La Motte , G. de Marino , G. De Nardo , G. De Pietro , R. de Sangro , M. Destefanis , S. Dey , R. Dhamija , A. Di Canto , F. Di Capua , J. Dingfelder , Z. Doležal , I. Domínguez Jiménez , T. V. Dong , X. Dong , M. Dorigo , D. Dossett , S. Dubey , K. Dugic , G. Dujany , P. Ecker , P. Feichtinger , T. Ferber , T. Fillinger , C. Finck , G. Finocchiaro , A. Fodor , F. Forti , B. G. Fulsom , A. Gabrielli , E. Ganiev , M. Garcia-Hernandez , R. Garg , G. Gaudino , V. Gaur , A. Gaz , A. Gellrich , G. Ghevondyan , D. Ghosh , H. Ghumaryan , G. Giakoustidis , R. Giordano , A. Giri , P. Gironella Gironell , A. Glazov , B. Gobbo , R. Godang , O. Gogota , P. Goldenzweig , W. Gradl , S. Granderath , E. Graziani , D. Greenwald , Z. Gruberová , Y. Guan , K. Gudkova , I. Haide , Y. Han , T. Hara , C. Harris , K. Hayasaka , H. Hayashii , S. Hazra , C. Hearty , M. T. Hedges , A. Heidelberg , I. Heredia de la Cruz , M. Hernández Villanueva , T. Higuchi , M. Hoek , M. Hohmann , R. Hoppe , P. Horak , C.-L. Hsu , T. Humair , T. Iijima , K. Inami , G. Inguglia , N. Ipsita , A. Ishikawa , R. Itoh , M. Iwasaki , D. Jacobi , W. W. Jacobs , D. E. Jaffe , E.-J. Jang , Q. P. Ji , S. Jia , Y. Jin , A. Johnson , K. K. Joo , H. Junkerkalefeld , M. Kaleta , A. B. Kaliyar , J. Kandra , K. H. Kang , S. Kang , G. Karyan , T. Kawasaki , F. Keil , C. Ketter , C. Kiesling , C.-H. Kim , D. Y. Kim , J.-Y. Kim , K.-H. Kim , Y.-K. Kim , K. Kinoshita , P. Kodyš , T. Koga , S. Kohani , K. Kojima , A. Korobov , S. Korpar , E. Kovalenko , R. Kowalewski , P. Križan , P. Krokovny , T. Kuhr , Y. Kulii , D. Kumar , R. Kumar , K. Kumara , T. Kunigo , A. Kuzmin , Y.-J. Kwon , S. Lacaprara , Y.-T. Lai , K. Lalwani , T. Lam , L. Lanceri , J. S. Lange , T. S. Lau , M. Laurenza , R. Lebourcher , F. R. Le Diberder , M. J. Lee , C. Lemettais , P. Leo , P. M. Lewis , C. Li , L. K. Li , Q. M. Li , W. Z. Li , Y. Li , Y. B. Li , Y. P. Liao , J. Libby , J. Lin , S. Lin , M. H. Liu , Q. Y. Liu , Y. Liu , Z. Q. Liu , D. Liventsev , S. Longo , T. Lueck , T. Luo , C. Lyu , Y. Ma , C. Madaan , M. Maggiora , S. P. Maharana , R. Maiti , G. Mancinelli , R. Manfredi , E. Manoni , M. Mantovano , S. Marcello , C. Marinas , C. Martellini , A. Martens , A. Martini , T. Martinov , L. Massaccesi , M. Masuda , D. Matvienko , S. K. Maurya , M. Maushart , J. A. McKenna , R. Mehta , F. Meier , D. Meleshko , M. Merola , C. Miller , M. Mirra , S. Mitra , K. Miyabayashi , H. Miyake , G. B. Mohanty , S. Mondal , S. Moneta , H.-G. Moser , R. Mussa , I. Nakamura , K. R. Nakamura , M. Nakao , Y. Nakazawa , M. Naruki , Z. Natkaniec , A. Natchii , M. Nayak , G. Nazaryan , M. Neu , S. Nishida , S. Ogawa , H. Ono , Y. Onuki , F. Otani , G. Pakhlova , E. Paoloni , S. Pardi , K. Parham , H. Park , J. Park , K. Park , S.-H. Park , B. Paschen , A. Passeri , S. Patra , T. K. Pedlar , I. Peruzzi , R. Peschke , R. Pestotnik , M. Piccolo , L. E. Piilonen , P. L. M. Podesta-Lerma , T. Podobnik , S. Pokharel , C. Praz , S. Prell , E. Prencipe , M. T. Prim , I. Prudiiev , H. Purwar , P. Rados , G. Raeuber , S. Raiz , N. Rauls , K. Ravindran , J. U. Rehman , M. Reif , S. Reiter , M. Remnev , L. Reuter , D. Ricalde Herrmann , I. Ripp-Baudot , G. Rizzo , S. H. Robertson , M. Roehrken , J. M. Roney , A. Rostomyan , N. Rout , D. A. Sanders , S. Sandilya , L. Santelj , V. Savinov , B. Scavino , S. Schneider

K. Trabelsi , I. Tsaklidis , I. Ueda , T. Uglov , K. Unger , Y. Unno , K. Uno , S. Uno , P. Urquijo ,
 Y. Ushiroda , S. E. Vahsen , R. van Tonder , K. E. Varvell , M. Veronesi , A. Vinokurova ,
 V. S. Vismaya , L. Vitale , V. Vobbiliseti , R. Volpe , M. Wakai , S. Wallner , M.-Z. Wang , Z. Wang ,
 A. Warburton , M. Watanabe , S. Watanuki , C. Wessel , J. Wiechczynski , E. Won , X. P. Xu ,
 B. D. Yabsley , S. Yamada , W. Yan , J. Yelton , J. H. Yin , K. Yoshihara , C. Z. Yuan , J. Yuan ,
 L. Zani , F. Zeng , B. Zhang , J. S. Zhou , Q. D. Zhou , L. Zhu , V. I. Zhukova , and R. Žlebčák 

(The Belle and Belle II Collaborations)

We present the first search for the lepton flavor-violating decay modes $B^0 \rightarrow K_S^0 \tau^\pm \ell^\mp$ ($\ell = \mu, e$) using the 711 fb $^{-1}$ and 365 fb $^{-1}$ data samples recorded by the Belle and Belle II detectors, respectively. We use a hadronic B -tagging technique, and search for the signal decay in the system recoiling against the fully reconstructed B meson. We find no evidence for $B^0 \rightarrow K_S^0 \tau^\pm \ell^\mp$ decays and set 90% confidence level upper limits on the branching fractions in the range of $[0.8, 3.6] \times 10^{-5}$.

Recent anomalies observed in semileptonic B decays, particularly in transitions like $b \rightarrow c \tau \nu$ [1], may indicate deviations from lepton flavor universality. According to this principle, the three generations of leptons are expected to interact identically with gauge bosons, except for mass differences. The experimental deviations from the standard model (SM) predictions suggest the potential existence of new heavy particles that couple preferentially to third-generation leptons. Recently, Belle II reported a $b \rightarrow s \nu \bar{\nu}$ excess and obtained the branching fraction $\mathcal{B}(B^+ \rightarrow K^+ \nu \bar{\nu}) = (2.3 \pm 0.7) \times 10^{-5}$ [2], which is 2.7 standard deviations (σ) larger than the SM expectation. If confirmed, this would not only be physics beyond the standard model (BSM), but could also reflect off-diagonal couplings between leptons of different flavors [3, 4]. Lepton flavor-violating (LFV) decays, which are forbidden in the SM, could then occur in B meson decays at significant rates. Ref.[4], starting from the $B^+ \rightarrow K^+ \nu \bar{\nu}$ excess, predicts an enhancement of $\mathcal{B}(B \rightarrow K \tau^\pm \mu^\mp)$ to $[2, 3] \times 10^{-6}$, which is close to the current experimental sensitivity. The BSM models in Refs. [3] and [5] predict significant enhancements in the branching fractions (\mathcal{B}) of processes such as $b \rightarrow s \tau \ell$, with the effect being enhanced due to the coupling of the third-generation b quark with the heaviest lepton, τ . This results in a notable increase in the branching fractions of $B \rightarrow K \tau^\pm \ell^\mp$ ($\ell = \mu, e$) decays and provides a potential experimental window into BSM physics.

BaBar performed the first LFV searches in $B^+ \rightarrow K^+ \tau^\pm \ell^\mp$ modes and set upper limits (ULs) on their branching fractions in the range of $[1.5, 4.5] \times 10^{-5}$ at 90% confidence level (CL) [6]. Belle provided the most stringent UL on the $B^+ \rightarrow K^+ \tau^+ \mu^-$ decay of 6×10^{-6} at 90% CL using 772×10^6 $B\bar{B}$ pairs [7], significantly better than LHCb's limit of 3.9×10^{-5} , obtained with 9 fb $^{-1}$ of pp collision data [8]. Moreover, LHCb set ULs on $B^0 \rightarrow K^{*0} \tau^\pm \mu^\mp$ decays in the range of $[0.8, 1.0] \times 10^{-5}$ at 90% CL [9].

In this Letter, we present the first search for the LFV decays $B^0 \rightarrow K_S^0 \tau^\pm \ell^\mp$ ($\ell = \mu, e$). We employ a hadronic B -tagging technique, and then use recoil mass to reconstruct the mass of the τ . Our results are based on a combined analysis of 772×10^6 $B\bar{B}$ pairs (711 fb $^{-1}$) from

Belle and 387×10^6 $B\bar{B}$ pairs (365 fb $^{-1}$) from Belle II (2019–2022). The advantage of K_S^0 over K^+ and K^{*0} in $B \rightarrow K \tau \ell$ decays is its very pure $K_S^0 \rightarrow \pi^+ \pi^-$ signature, which is an additional advantage over pp collision experiments, highlighting the unique strengths of Belle and Belle II.

Belle operated at the KEKB asymmetric-energy collider with electron-(positron)-beam energies of 8.0(3.5) GeV [10]. Belle II operates at the successor, SuperKEKB, designed to deliver forty times higher instantaneous luminosity than KEKB, with electron-(positron)-beam energies of 7(4) GeV [11]. The Belle II detector [13] is a upgraded version of the Belle [12], including a vertex detector (VXD), composed of two inner layers of pixel detectors (PXD) and four outer layers of double-sided strip detectors (SVD), a central drift chamber (CDC), a time-of-propagation (TOP) detector in the central detector volume and an aerogel ring-imaging Cherenkov (ARICH) detector in the forward region, and an electromagnetic calorimeter (ECL). All these sub-detectors are located inside the same solenoid as in Belle, with a K_L^0 -Muon detector (KLM) instrumented in the yoke.

The analysis procedure is first developed using simulation before being applied to data. EvtGen [14] is used to generate $e^+ e^- \rightarrow \Upsilon(4S) \rightarrow B\bar{B}$ with final-state radiation simulated by PHOTOS [15]. The $B^0 \rightarrow K_S^0 \tau^\pm \ell^\mp$ signal channels are modeled using an uniform three-body phase space model. The KKMC [16] and PYTHIA [17] packages are used to simulate the $e^+ e^- \rightarrow q\bar{q}$ continuum ($q = u, d, s, c$). The detector responses are modeled by GEANT3 [18] for Belle and GEANT4 [19] for Belle II. We use the Belle II analysis software framework (basf2) [20] to reconstruct the events for both Belle and Belle II data. The Belle data is converted to the Belle II format for basf2 compatibility using the B2BII framework [21].

In each $B\bar{B}$ pair, if one B meson, B_{sig} , decays to a final state involving neutrinos, it cannot be fully reconstructed as neutrinos escape the detector. However, the presence of missing energy and momentum can be inferred from the other B meson. This process is called tagging, with the other B meson referred to as B_{tag} . By combining the visible particles from B_{sig} , we can kine-

matically constrain the undetected neutrinos as possible products of a τ decay. We require a fully reconstructed B_{tag} using the full-event-interpretation (FEI) algorithm [22], a machine-learning based algorithm developed for B -tagging analyses at Belle and Belle II. Each reconstructed B_{tag} candidate is assigned a multivariate classifier output, \mathcal{P}_{FEI} , ranging from zero (background-like) to one (signal-like). To constrain the B_{tag} kinematics, we require the beam-energy-constrained mass $M_{\text{bc}} = \sqrt{(E_{\text{beam}}/c^2)^2 - (p_{B_{\text{tag}}}/c)^2} > 5.27 \text{ GeV}/c^2$, and the energy difference $\Delta E = E_{B_{\text{tag}}} - E_{\text{beam}}$ to satisfy $-0.15 < \Delta E < 0.1 \text{ GeV}$. Here, E_{beam} , $E_{B_{\text{tag}}}$, and $p_{B_{\text{tag}}}$ denote the beam energy, and the energy and momentum of the B_{tag} candidate in the e^+e^- center-of-mass (c.m.) frame, respectively. If multiple B_{tag} candidates are reconstructed in a single event, the one with the highest \mathcal{P}_{FEI} is chosen, and candidates satisfying $\mathcal{P}_{\text{FEI}} > 0.001$ are retained. Using these criteria, the B -tagging has an average efficiency of 0.59% and a purity of 44%. Here, purity is the ratio of reconstructed or expected signal events to total events in the signal region.

Tracks and clusters not associated to B_{tag} are used to reconstruct the B_{sig} , whose flavor is assumed to be opposite to that of the B_{tag} candidate. The BSM couplings between $b\tau$ and $b\ell$, or between $s\tau$ and $s\ell$, can be different, leading to an asymmetric differential decay rate between $b \rightarrow s\tau^+\ell^-$ and $b \rightarrow s\tau^-\ell^+$ (see Eq. 9 in Ref. [3]). To address this and the different background characteristics, we distinguish signal channels by the primary lepton charge and b quark flavor: same-sign SS_ℓ ($B^0 \rightarrow K_S^0\tau^-\ell^+$) and opposite-sign OS_ℓ ($B^0 \rightarrow K_S^0\tau^+\ell^-$). Due to B^0 - \bar{B}^0 mixing, a small fraction (χ_d) [23] of SS_ℓ decays are classified as OS_ℓ decays, and vice versa. The τ candidates are reconstructed via $\tau \rightarrow e\nu\bar{\nu}$, $\mu\nu\bar{\nu}$, $\pi\nu$, or $\rho(\rightarrow\pi\pi^0)\nu$, covering over 70% of τ decays [23]. Signal channels are formed by combining a K_S^0 , a primary lepton (ℓ), and a τ decay track (t_τ).

We reconstruct K_S^0 candidates from a pair of oppositely charged tracks assumed to be pions, with a common vertex. We use a standard momentum-binned K_S^0 selection that includes requirements on the K_S^0 flight information [24]. The purity of the K_S^0 candidates exceeds 98%, with backgrounds predominantly containing real K_S^0 candidates.

To select ℓ and t_τ , we require the transverse (d_0) and longitudinal (z_0) projection of the distance of closest approach to the origin to be less than 0.5 cm and 5.0 cm to reduce misreconstructed or spurious tracks from beam-induced background. At least 20 hits in the CDC are required. For Belle, we use information from the KLM only to identify muon candidates, while for Belle II, we use information from all sub-detectors except the VXD. Muon candidates are required to have momenta greater than 0.6 GeV/ c to sufficiently penetrate the KLM. This selection has an efficiency of 89% with a pion misidentification rate lower than 2.5% for both samples [25]. Electrons are required to have momenta greater than 0.3 GeV/ c to lie in the acceptance of the ECL. For Belle, electrons

are identified using the information from the ECL, CDC and aerogel threshold Cerenkov counter (ACC), respectively. For Belle II, the electron identification uses a boosted-decision-tree (BDT) classifier trained with information from all sub-detectors except the VXD. The electron identification has an efficiency of 92% (86%) and a pion misidentification rate below 0.3% (0.5%) for Belle (Belle II) [26]. To recover electron candidates with bremsstrahlung, we accept photons with a minimum energy of 50 MeV that are within a 50 mrad angle of an electron track. Pion candidates for t_τ reconstruction are selected using PID likelihoods using information from the ACC, CDC, and time-of-flight scintillation counters for Belle. For Belle II, information from all the subdetectors except the VXD is used. This achieves a pion identification efficiency of 85% (83%) and a kaon misidentification rate of 6% (8%) for Belle (Belle II).

The $\tau \rightarrow \rho(\rightarrow\pi\pi^0)\nu$ mode, the most probable τ decay channel ($\mathcal{B} > 20\%$), has never been used in $B \rightarrow K\tau\ell$ analyses [6–8]. Understanding this mode is crucial for improving the kinematic properties of t_τ and enhancing background rejection strategies. However, its reconstruction is challenging due to contamination from π^0 mesons, which can be misreconstructed using either a fake photon (clusters associated with hadronic deposits) or a photon from beam-background. To reconstruct the clean $\tau \rightarrow \rho\nu$ mode, photons are selected with energies above 50(60) MeV, 100(75) MeV, and 150(100) MeV in the barrel, forward, and backward endcaps for Belle (Belle II). We developed classifiers to suppress these backgrounds using BDTs. The common cluster features are energy, polar angle (relative to the beam-pipe), lateral energy distribution [27], distance between the cluster and its nearest track, and fraction of cluster energy detected in the central part. For Belle II classifiers, we include additional features: the time-difference between the collision and reconstructed cluster; outputs of classifiers using eleven Zernike moments [28]; and identifiers for electromagnetic or hadronic showers using pulse shape discrimination [29]. For Belle, additional features include azimuthal angle, number of crystals in the cluster, and energy in the most energetic crystal. On average, the classifiers reduce backgrounds by 90% with a π^0 efficiency of 70%, including the selection $0.125 < M_{\pi^0} < 0.145 \text{ GeV}/c^2$. The ρ candidates are selected with $0.60 < M_{\pi\pi^0} < 0.94 \text{ GeV}/c^2$, with one candidate randomly chosen due to the multiplicity of 1.07.

The rest-of-event (ROE) consists of the tracks and clusters not used in B_{tag} and B_{sig} . We select events without any track in the ROE having $|d_0| < 10 \text{ cm}$ and $|z_0| < 20 \text{ cm}$. The ROE clusters are required to satisfy the same selection criteria as the photons used for π^0 reconstruction. If the t_τ candidate is identified with multiple particle hypotheses, we assign a single one according to the following priority order (based on the purity of the modes): muon, electron, and pion. We require the $\tau \rightarrow \pi\nu$ mode to have no additional π^0 candidate in the ROE to avoid double counting with the $\tau \rightarrow \rho\nu$ mode.

The B_{sig} momentum is equal in magnitude and opposite in direction to that of B_{tag} , $\vec{p}_{B_{\text{tag}}}$, and the B_{sig} energy is equal to E_{beam} in the c.m. frame. Therefore, the τ momentum and energy are given by,

$$\begin{aligned}\vec{p}_\tau &= -\vec{p}_{B_{\text{tag}}} - \vec{p}_{K_S^0} - \vec{p}_\ell, \\ E_\tau &= E_{\text{beam}} - E_{K_S^0} - E_\ell,\end{aligned}$$

from which we reconstruct the recoiling M_τ according to Eq. 1. The signal yields are then extracted from M_τ , as signal events peak at the known τ mass [23], while the background remains flat without any peaking structures in the simulation. When t_τ is μ or e (i.e. when there are two leptons in B_{sig}), it is possible to form both SS_ℓ and OS_ℓ candidates, but this does not bias the signal yield as misassigned candidates do not peak in M_τ .

$$M_{\text{recoil}} = M_\tau = \left[m_B^2 + M_{K_S^0 \ell}^2 - 2 \left(E_{\text{beam}} E_{K_S^0 \ell} + |\vec{p}_{B_{\text{tag}}}||\vec{p}_{K_S^0 \ell}| \cos \theta \right) \right]^{\frac{1}{2}} \quad (1)$$

Here, m_B is the known B^0 mass [23]; $M_{K_S^0 \ell}$, $E_{K_S^0 \ell}$, $\vec{p}_{K_S^0 \ell}$ are the mass, energy, and momentum of the system composed of the K_S^0 and ℓ , respectively; θ is the angle between $\vec{p}_{B_{\text{tag}}}$ and $\vec{p}_{K_S^0 \ell}$. The M_τ resolution is approximately 25 MeV/ c^2 for both Belle and Belle II simulations.

The background after the pre-selection is mainly decays arising from $b \rightarrow c$ transitions. Events with $B^0 \rightarrow D^{(*)-} (\rightarrow K_S^0 t^- X) \ell^+ \nu$ decays, where the reconstructed primary lepton originates from semileptonic B^0 decay and a track t^- from $D^{(*)-}$ is misinterpreted as coming from the τ decay, with X representing any other particles, constitute the dominant source of background in SS_ℓ modes. If $B^0 \rightarrow D^{(*)-} \ell^+ \nu$ undergoes a flavor transformation due to B^0 - \bar{B}^0 mixing, this results in a change in the signs of the final states ($\bar{B}^0 \rightarrow D^{(*)+} \ell^- \bar{\nu}$) and provides the appropriate sign configuration for the final state in OS_ℓ modes. Additionally, the reconstruction of the primary lepton from B_{sig} tends to favor a higher momentum lepton originating from the B^0 meson. Consequently, semileptonic B decays are the primary background in both SS_ℓ and OS_ℓ modes. As the K_S^0 and t_τ come from a D meson, we require the invariant mass of K_S^0 and t_τ to be greater than 1.91 GeV/ c^2 , i.e., greater than the D meson mass accounting for resolution. For $\tau \rightarrow \rho \nu$ decay, we require $M_{K_S^0 \rho}$ to be greater than 2.1 GeV/ c^2 due to the poor mass resolution resulting from the presence of a π^0 candidate. Because $B^0 \rightarrow K_S^0 J/\psi (\rightarrow \ell^+ \ell^-)$ background can pass our selection criteria, events in the range $3.00 < M_{t_\tau \ell} < 3.14$ GeV/ c^2 are rejected when ℓ is an electron (muon) for the $\tau \rightarrow e(\mu) \nu \bar{\nu}$ mode. To suppress the photon conversion background, we require $M_{t_\tau \ell}$, in this case $M_{e^+ e^-}$, to be greater than 0.15 GeV/ c^2 .

Continuum $q\bar{q}$ events can be distinguished from $B\bar{B}$ events by exploiting their difference in event topologies.

We use sphericity-related variables [30] and require the cosine of the angle between the thrust axis of B_{tag} and the other particles not used in B_{tag} ($\cos \theta_T$) to be less than 0.9. These selections reduce the $q\bar{q}$ background by 86% and retain 88% of the signal for both samples.

After the above selection criteria, the background consists of charm meson semileptonic decays with a K_S^0 and ℓ in their final state, other $B\bar{B}$ decays, and $q\bar{q}$ events. For each signal mode, BDT classifiers are trained with 11 features to suppress the residual backgrounds. These features include $M_{K_S^0 \ell}$, which helps to suppress the background from charm meson semileptonic decays, the sum of ECL cluster energies in the ROE, energies of the ℓ and t_τ , event-shape variables and modified Fox-Wolfram moments [31], which help to reduce the $q\bar{q}$ background. The same BDT output criterion are used for Belle and Belle II because of the similar performance, determined using figure of merit $\epsilon_{\text{sig}} / (a + \sqrt{N_{\text{bkg}}})$ [32]. Here, ϵ_{sig} is the signal efficiency, N_{bkg} is the expected background yield and $a = 3$ represents the target significance in terms of standard deviations. The BDT selection results in an average signal efficiency of about 75% and rejects 90% of the remaining background.

The purity in the simulations is similar in Belle and Belle II for every channel after applying all selection criteria, so the two datasets are merged. To extract the signal yield, we do a single unbinned-maximum-likelihood fit to the M_τ distribution of the combined dataset. The probability density function (PDF) used to model the M_τ signal distribution is a Johnson function [33]. The parameters that describe the signal shape are fixed to the values obtained from the fit to the simulated samples. Background events have a smooth distribution in the M_τ fit region, modeled using a second-order polynomial. To validate the fitting procedure, we generate large ensembles of simulated experiments, in which the M_τ distributions are produced from the PDFs used for fitting. Comparisons of the simulated and measured signal yields indicate no obvious bias.

The $B^0 \rightarrow D^- \pi^+$ sample is used to calibrate B_{tag} efficiency. We reconstruct B_{tag} using the FEI and a high momentum π^+ , then compute M_{recoil} to observe the D signal using Eq. 1. The yield ratio $\mathcal{R}_{\text{FEI}} = N_{\text{data}} / N_{\text{simulation}} = 0.74 \pm 0.04$ (0.81 ± 0.04) is taken as the calibration factor for the B_{tag} efficiency in Belle (Belle II).

The $B^0 \rightarrow D_s^+ D^-$ sample is used to calibrate the signal PDF and BDT selections. The D^- mass is reconstructed similarly to the τ mass in the signal decays. We reconstruct neutral B_{tag} candidates using the FEI algorithm and D_s^+ , sharing the same momentum range as $K_S^0 \ell$, through the decays $\phi (\rightarrow K^+ K^-) \pi^+$ and $K_S^0 K^+$ and a charged track from D as t_τ . The distribution of the mass recoiling against the B_{tag} and D_s^+ system is shown in Fig. 1 and clear signals for D^- and D^{*-} are visible. The $B^0 \rightarrow D_s^+ D^{*-}$ component is also fitted but we do not use it due to its lower purity. The $B^0 \rightarrow D_s^+ D^-$ signal PDF is modeled by the Johnson function and the parameters are fixed in the fits, except the mean, while

the background is described by an exponential function with floating yield and shape parameters. We introduce a scale factor f to account for data-simulation difference on the width from signal simulation. The f ratio, determined to be 1.04 ± 0.15 , is used as a correction factor for the width. The value of $\mathcal{B}(B^0 \rightarrow D_s^+ D^-)$ is measured to be $(10.1 \pm 1.2) \times 10^{-3}$, consistent with the world-average value [23] within 2σ , and serves as a closure test of the entire analysis chain. To validate the BDT performance, we apply $B^0 \rightarrow K_S^0 \tau^\pm \ell^\mp$ weights to $B^0 \rightarrow D_s^+ D^-$ events. The efficiency is derived from $B^0 \rightarrow D_s^+ D^-$ yields before and after BDT selection using M_{recoil} fits. The data-simulation efficiency ratios (\mathcal{R}_{BDT}) are 0.93 ± 0.17 , 0.96 ± 0.16 , 0.92 ± 0.16 , and 0.96 ± 0.18 for the OS_μ , SS_μ , OS_e , and SS_e modes, respectively.

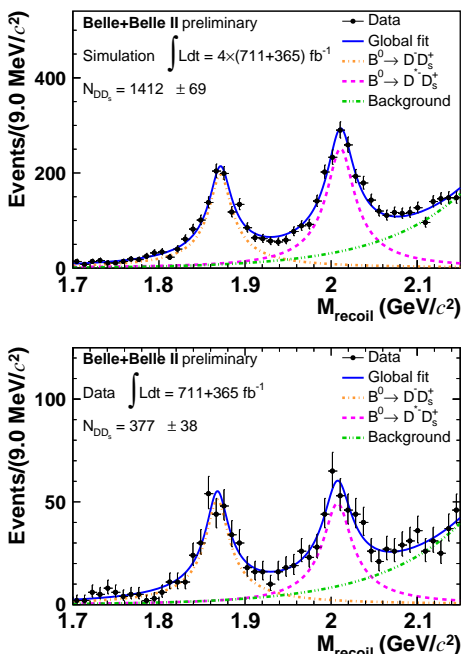


FIG. 1. Fit to the recoil mass of the B_{tag} and D_s^+ system for simulation (upper) and data (lower) with the combined Belle and Belle II samples.

Figure 2 shows the M_τ fits to data for $B^0 \rightarrow K_S^0 \tau^\pm \ell^\mp$ decays. There is no significant signal in any of the fit channels. We translate the number of observed events N_{sig} into a branching fraction \mathcal{B} using the expression

$$\mathcal{B} = \frac{N_{\text{sig}}}{\epsilon \times 2N_{B\bar{B}} \times (1 + f_{+-}/f_{00})^{-1}}, \quad (2)$$

where ϵ is the efficiency after \mathcal{R}_{BDT} and \mathcal{R}_{FEI} calibrations. The efficiency also includes the branching fractions of K_S^0 , τ , ρ , π^0 , and the effect of B^0 - \bar{B}^0 mixing (i.e. signal loss in mixed events) in the simulation. In the case where the true branching fractions are zero, the resulting estimates are unbiased. We use $N_{B\bar{B}} = 1159 \times 10^6$, which is the total number of $B\bar{B}$ pairs for the combined datasets; and $f_{+-}/f_{00} = 1.052 \pm 0.031$, which is the ratio

of $\mathcal{B}(\Upsilon(4S) \rightarrow B^+ B^-)$ to $\mathcal{B}(\Upsilon(4S) \rightarrow B^0 \bar{B}^0)$ [34].

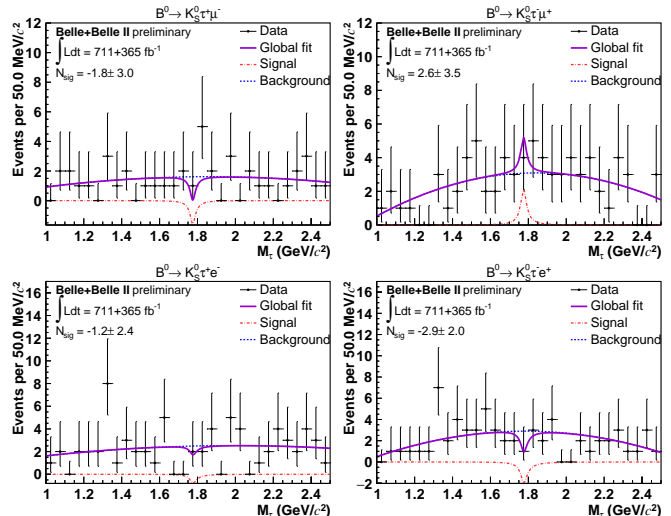


FIG. 2. The M_τ distributions and fits for the combined Belle and Belle II datasets. The black dots with error bars show the data, the red dash-dotted curve shows the signal component, the blue dashed curve shows the background component, and the purple solid curve shows the global fit.

We obtain ULs on the signal yields using pseudo-experiments. They are generated using background and signal PDFs for different values of the signal branching fractions, performing 10,000 fits for each value. We then define $N_{\text{sig}}^{\text{UL}}$ at 90% CL as the signal yield for which 10% of the experiments have fit yields less than the observed N_{sig} in data. Systematic uncertainties are included by smearing the N_{sig} distribution obtained from the pseudo-experiments with the fractional systematic uncertainty, which has an effect of less than 1% on the mean N_{sig} . The ULs on the branching fractions \mathcal{B}^{UL} are then obtained from $N_{\text{sig}}^{\text{UL}}$ using Eq. 2. Including the effect of B^0 - \bar{B}^0 mixing in the efficiency (Eq. 2) ensures ULs correctly cover the case of zero true branching fractions and are conservative otherwise. Table I summarizes the efficiency, fit results, and observed ULs at 90% CL for the four channels. Expected ULs, derived from the no-signal assumption, are in the range $[2.1, 2.2] \times 10^{-5}$.

TABLE I. Efficiencies (ϵ), signal yields (N_{sig}) of the data fit, central value of the branching fractions and the observed \mathcal{B}^{UL} at 90% CL. The first uncertainty of the central value is statistical and the second is systematic.

Channels	$\epsilon(10^{-4})$	N_{sig}	$\mathcal{B}(10^{-5})$	
			Central value	UL
$B^0 \rightarrow K_S^0 \tau^+ \mu^-$	1.7	-1.8 ± 3.0	$-1.0 \pm 1.6 \pm 0.2$	1.1
$B^0 \rightarrow K_S^0 \tau^- \mu^+$	2.1	2.6 ± 3.5	$1.1 \pm 1.6 \pm 0.3$	3.6
$B^0 \rightarrow K_S^0 \tau^+ e^-$	2.0	-1.2 ± 2.4	$-0.5 \pm 1.1 \pm 0.1$	1.5
$B^0 \rightarrow K_S^0 \tau^- e^+$	2.1	-2.9 ± 2.0	$-1.2 \pm 0.9 \pm 0.3$	0.8

The primary source of systematic uncertainty arises

from the BDT selections, which is 16–18%, based on the uncertainty in \mathcal{R}_{BDT} using the $B^0 \rightarrow D_s^+ D^-$ sample. Using the same sample, the uncertainty from the signal PDF is 15%. This includes the uncertainties in width (uncertainty of the width correction factor), mean (deviation from nominal D mass in the data fit), skewness, and Gaussian component strength of the Johnson function, estimated using a new PDF reweighted by mode-dependent calibration factors for the dominant B -tagging modes. The uncertainty in the B_{tag} efficiency is taken from the uncertainty of \mathcal{R}_{FEI} (4%). The small difference (0.8–1.6%) in the validation of the fitting procedure is treated as the associated uncertainty. The uncertainty in K_S^0 reconstruction is estimated to be 1.1% using a $D^{*+} \rightarrow \pi^+ D^0, D^0 \rightarrow K_S^0 \pi^+ \pi^-$ sample. The Belle PID uncertainties are evaluated using $J/\psi \rightarrow \ell^+ \ell^-$ and $D^{*+} \rightarrow D^0(\rightarrow K^- \pi^+) \pi^+$ samples to be 0.3%, 0.4% and 1.0% for muons, electrons, and pions, respectively. The Belle II PID uncertainties for muon, electron and pion are 0.5%, 1.0% and 1.0%, respectively, which are obtained using the samples described in Ref. [35]. The uncertainty from the π^0 reconstruction is 1.3% using $B^+ \rightarrow K^{*+}(\rightarrow K^+ \pi^0) J/\psi$ and $D^{*-} \rightarrow \bar{D}^0(\rightarrow K^+ \pi^- \pi^0) \pi^-$ samples. The uncertainty for the requirement that there is no additional π^0 candidate in the ROE in the $\tau \rightarrow \pi \nu$ mode is 1.0% using $B_{\text{tag}} B(\rightarrow K_S^0 J/\psi)$ events. The uncertainties arising from $N_{B\bar{B}}, f_{+-}/f_{00}$, and the branching fractions of K_S^0, τ, ρ and π^0 decays [23] are 1.1%, 1.5% and 0.7%, respectively. For sources with different systematic uncertainties in Belle and Belle II, we calculate the total multiplicative values by weighting the individual uncertainties according to the integrated luminosities of the two samples. The total systematic uncertainties are 24%, 22%, 23%, and 24% for $OS_\mu, SS_\mu, OS_e,$ and SS_e modes, respectively.

In summary, we have searched for $B^0 \rightarrow K_S^0 \tau^\pm \ell^\mp$ for the first time using Belle and Belle II datasets. This is also the first direct search for LFV in B decays using the Belle II dataset. The ULs on the branching fractions at 90% CL are:

$$\begin{aligned} \mathcal{B}(B^0 \rightarrow K_S^0 \tau^+ \mu^-) &< 1.1 \times 10^{-5} \\ \mathcal{B}(B^0 \rightarrow K_S^0 \tau^- \mu^+) &< 3.6 \times 10^{-5} \\ \mathcal{B}(B^0 \rightarrow K_S^0 \tau^+ e^-) &< 1.5 \times 10^{-5} \\ \mathcal{B}(B^0 \rightarrow K_S^0 \tau^- e^+) &< 0.8 \times 10^{-5} \end{aligned}$$

The results for $B^0 \rightarrow K_S^0 \tau^\pm e^\mp$ are the most stringent ULs on $b \rightarrow s \tau e$ transitions, and those for $B^0 \rightarrow K_S^0 \tau^\pm \mu^\mp$ are among the best limits on $b \rightarrow s \tau \mu$ transitions achieved to date. These results are approaching the potential BSM enhancement level of $\mathcal{O}(10^{-6})$. Additionally, we provide the selection efficiency as a function of $(M_{\tau\ell}^2, M_{K_S^0\ell}^2)$ in the Supplemental Material, to allow these results to be reinterpreted in specific BSM models.

ACKNOWLEDGMENTS

This work, based on data collected using the Belle II detector, which was built and commissioned prior to March 2019, and data collected using the Belle detector, which was operated until June 2010, was supported by Higher Education and Science Committee of the Republic of Armenia Grant No. 23LCG-1C011; Australian Research Council and Research Grants No. DP200101792, No. DP210101900, No. DP210102831, No. DE220100462, No. LE210100098, and No. LE230100085; Austrian Federal Ministry of Education, Science and Research, Austrian Science Fund No. P 34529, No. J 4731, No. J 4625, and No. M 3153, and Horizon 2020 ERC Starting Grant No. 947006 ‘‘InterLeptons’’; Natural Sciences and Engineering Research Council of Canada, Compute Canada and CANARIE; National Key R&D Program of China under Contract No. 2022YFA1601903, National Natural Science Foundation of China and Research Grants No. 11575017, No. 11761141009, No. 11705209, No. 11975076, No. 12135005, No. 12150004, No. 12161141008, No. 12475093, and No. 12175041, and Shandong Provincial Natural Science Foundation Project ZR2022JQ02; the Czech Science Foundation Grant No. 22-18469S and Charles University Grant Agency project No. 246122; European Research Council, Seventh Framework PIEF-GA-2013-622527, Horizon 2020 ERC-Advanced Grants No. 267104 and No. 884719, Horizon 2020 ERC-Consolidator Grant No. 819127, Horizon 2020 Marie Sklodowska-Curie Grant Agreement No. 700525 ‘‘NIOBE’’ and No. 101026516, and Horizon 2020 Marie Sklodowska-Curie RISE project JENNIFER2 Grant Agreement No. 822070 (European grants); L’Institut National de Physique Nucléaire et de Physique des Particules (IN2P3) du CNRS and L’Agence Nationale de la Recherche (ANR) under grant ANR-21-CE31-0009 (France); BMBF, DFG, HGF, MPG, and AvH Foundation (Germany); Department of Atomic Energy under Project Identification No. RTI 4002, Department of Science and Technology, and UPES SEED funding programs No. UPES/R&D-SEED-INFRA/17052023/01 and No. UPES/R&D-SOE/20062022/06 (India); Israel Science Foundation Grant No. 2476/17, U.S.-Israel Binational Science Foundation Grant No. 2016113, and Israel Ministry of Science Grant No. 3-16543; Istituto Nazionale di Fisica Nucleare and the Research Grants BELLE2, and the ICSC – Centro Nazionale di Ricerca in High Performance Computing, Big Data and Quantum Computing, funded by European Union – NextGenerationEU; Japan Society for the Promotion of Science, Grant-in-Aid for Scientific Research Grants No. 16H03968, No. 16H03993, No. 16H06492, No. 16K05323, No. 17H01133, No. 17H05405, No. 18K03621, No. 18H03710, No. 18H05226, No. 19H00682, No. 20H05850, No. 20H05858, No. 22H00144, No. 22K14056, No. 22K21347, No. 23H05433, No. 26220706, and

No. 26400255, and the Ministry of Education, Culture, Sports, Science, and Technology (MEXT) of Japan; National Research Foundation (NRF) of Korea Grants No. 2016R1-D1A1B-02012900, No. 2018R1-A6A1A-06024970, No. 2021R1-A6A1A-03043957, No. 2021R1-F1A-1060423, No. 2021R1-F1A-1064008, No. 2022R1-A2C-1003993, No. 2022R1-A2C-1092335, No. RS-2023-00208693, No. RS-2024-00354342 and No. RS-2022-00197659, Radiation Science Research Institute, Foreign Large-Size Research Facility Application Supporting project, the Global Science Experimental Data Hub Center, the Korea Institute of Science and Technology Information (K24L2M1C4) and KREONET/GLORIAD; Universiti Malaya RU grant, Akademi Sains Malaysia, and Ministry of Education Malaysia; Frontiers of Science Program Contracts No. FOINS-296, No. CB-221329, No. CB-236394, No. CB-254409, and No. CB-180023, and SEP-CINVESTAV Research Grant No. 237 (Mexico); the Polish Ministry of Science and Higher Education and the National Science Center; the Ministry of Science and Higher Education of the Russian Federation and the HSE University Basic Research Program, Moscow; University of Tabuk Research Grants No. S-0256-1438 and No. S-0280-1439 (Saudi Arabia), and King Saud University, Riyadh, Researchers Supporting Project number (RSPD2024R873) (Saudi Arabia); Slovenian Research Agency and Research Grants No. J1-9124 and No. P1-0135; Ikerbasque, Basque Foundation for Science, the State Agency for Research of the Spanish Ministry of Science and Innovation through Grant No. PID2022-136510NB-C33, Agencia Estatal de Investigacion, Spain Grant No. RYC2020-029875-I and Generalitat

Valenciana, Spain Grant No. CIDEAGENT/2018/020; the Swiss National Science Foundation; The Knut and Alice Wallenberg Foundation (Sweden), Contracts No. 2021.0174 and No. 2021.0299; National Science and Technology Council, and Ministry of Education (Taiwan); Thailand Center of Excellence in Physics; TUBITAK ULAKBIM (Turkey); National Research Foundation of Ukraine, Project No. 2020.02/0257, and Ministry of Education and Science of Ukraine; the U.S. National Science Foundation and Research Grants No. PHY-1913789 and No. PHY-2111604, and the U.S. Department of Energy and Research Awards No. DE-AC06-76RLO1830, No. DE-SC0007983, No. DE-SC0009824, No. DE-SC0009973, No. DE-SC0010007, No. DE-SC0010073, No. DE-SC0010118, No. DE-SC0010504, No. DE-SC0011784, No. DE-SC0012704, No. DE-SC0019230, No. DE-SC0021274, No. DE-SC0021616, No. DE-SC0022350, No. DE-SC0023470; and the Vietnam Academy of Science and Technology (VAST) under Grants No. NVCC.05.12/22-23 and No. DL0000.02/24-25.

These acknowledgements are not to be interpreted as an endorsement of any statement made by any of our institutes, funding agencies, governments, or their representatives.

We thank the SuperKEKB team for delivering high-luminosity collisions; the KEK cryogenics group for the efficient operation of the detector solenoid magnet and IBelle on site; the KEK Computer Research Center for on-site computing support; the NII for SINET6 network support; and the raw-data centers hosted by BNL, DESY, GridKa, IN2P3, INFN, PNNL/EMSL, and the University of Victoria.

-
- [1] U. Florian *et al.*, *Rev. Mod. Phys.* **94**, 015003 (2022).
 [2] I. Adachi *et al.* (Belle II Collaboration), *Phys. Rev. D* **109**, 112006 (2024).
 [3] D. Becirević, O. Sumensari, and R. Zukanovich Funchal, *Eur. Phys. J. C* **76**, 134 (2016).
 [4] L. Allwicher *et al.*, *Phys. Lett. B* **848**, 138411 (2024).
 [5] S. L. Glashow, D. Guadagnoli, and K. Lane, *Phys. Rev. Lett.* **114**, 091801 (2015).
 [6] J. P. Lees *et al.* (BABAR Collaboration), *Phys. Rev. D* **86**, 012004 (2012).
 [7] S. Watanuki *et al.* (Belle Collaboration), *Phys. Rev. Lett.* **130**, 261802 (2023).
 [8] R. Aaij *et al.* (LHCb Collaboration), *J. High Energy Phys.* **06** **2020** 129.
 [9] R. Aaij *et al.* (LHCb Collaboration), *J. High Energy Phys.* **06** **2023** 143.
 [10] S. Kurokawa and E. Kikutani, *Nucl. Instrum. Methods Phys. Res., Sect. A* **499**, 1 (2003). T. Abe *et al.*, *Prog. Theor. Exp. Phys.* (2013) 03A001-03A011.
 [11] K. Akai, K. Furukawa, and H. Koiso, *Nucl. Instrum. Methods Phys. Res., Sect. A* **907**, 188 (2018).
 [12] A. Abashian *et al.* (Belle Collaboration), *Nucl. Instrum. Methods Phys. Res., Sect. A* **479**, 117 (2002).
 [13] T. Abe *et al.* (Belle II Collaboration), arXiv:1011.0352 (2010).
 [14] D. J. Lange, *Nucl. Instrum. Methods Phys. Res., Sect. A* **462**, 152 (2001).
 [15] E. Barberio and Z. Was, *Comp. Phys. Commun.* **79**, 291 (1994).
 [16] B. Ward, S. Jadach and Z. Was, *Nucl. Phys. B Proc. Suppl.* **116**, 73 (2003).
 [17] T. Sjöstrand *et al.*, *Comput. Phys. Commun.* **178**, 852 (2008).
 [18] R. Brun *et al.*, CERN-DD-EE-84-01 (1987).
 [19] S. Agostinelli *et al.*, *Nucl. Instrum. Methods Phys. Res., Sect. A* **506**, 250 (2003).
 [20] T. Kuhr *et al.* (Belle II Collaboration), *Comput. Software Big Sci.* **3**, 1 (2019).
 [21] M. Gelb *et al.*, *Comput. Software Big Sci.* **2**, 9 (2018).
 [22] T. Keck *et al.*, *Comput. Software Big Sci.* **1**, 6 (2019).
 [23] S. Navas *et al.* (Particle Data Group), *Phys. Rev. D* **110**, 030001 (2024).
 [24] E. Won *et al.* (Belle Collaboration), *Phys. Rev. D* **80**, 111101(R) (2009).
 [25] E. Nakano, *Nucl. Instrum. Methods Phys. Res., Sect. A* **494**, 402 (2002).

- [26] K. Hanagaki, H. Kakuno, H. Ikeda, T. Iijima, and T. Tsukamoto, Nucl. Instrum. Methods Phys. Res., Sect. A **485**, 490 (2002).
- [27] D. N. Brown, J. Ilic, and G. B. Mohanty, Nucl. Instrum. Methods Phys. Res., Sect. A **592**, 254 (2008).
- [28] A. Khotanzad and Y. Hong, IEEE Trans. Pattern Anal. Mach. Intell. **12**, 489 (1990).
- [29] S. Longo *et al.*, Nucl. Instrum. Methods Phys. Res., Sect. A **982**, 164562 (2020).
- [30] J. D. Bjorken and S. J. Brodsky, Phys. Rev. D **1**, 1416 (1970).
- [31] S. H. Lee *et al.* (Belle Collaboration), Phys. Rev. Lett. **91**, 261801 (2003).
- [32] G. Punzi, eConf **C030908**, MODT002 (2003).
- [33] N. L. Johnson, Biometrika **36**, 149 (1949).
- [34] Sw. Banerjee *et al.* (Heavy Flavor Averaging Group), arXiv:2411.18639.
- [35] L. Aggarwal *et al.* (Belle II Collaboration), Phys. Rev. Lett. **131**, 051804 (2023).

Supplemental material

SUPPLEMENTAL FIGURES

Figure 1 presents the selection efficiencies for the four signal modes: $B^0 \rightarrow K_S^0 \tau^+ \mu^-$, $B^0 \rightarrow K_S^0 \tau^- \mu^+$, $B^0 \rightarrow K_S^0 \tau^+ e^-$, and $B^0 \rightarrow K_S^0 \tau^- e^+$. The efficiency is shown as a function of two kinematic variables, $M_{\tau\ell}^2$ and $M_{K_S^0\ell}^2$, where the 4-momentum of the τ lepton is inferred using the B_{tag} reconstruction. These distributions can be utilized to reinterpret the results for different models and kinematics, extending beyond the uniform phase space distribution assumed in the signal simulation and upper limit estimation.

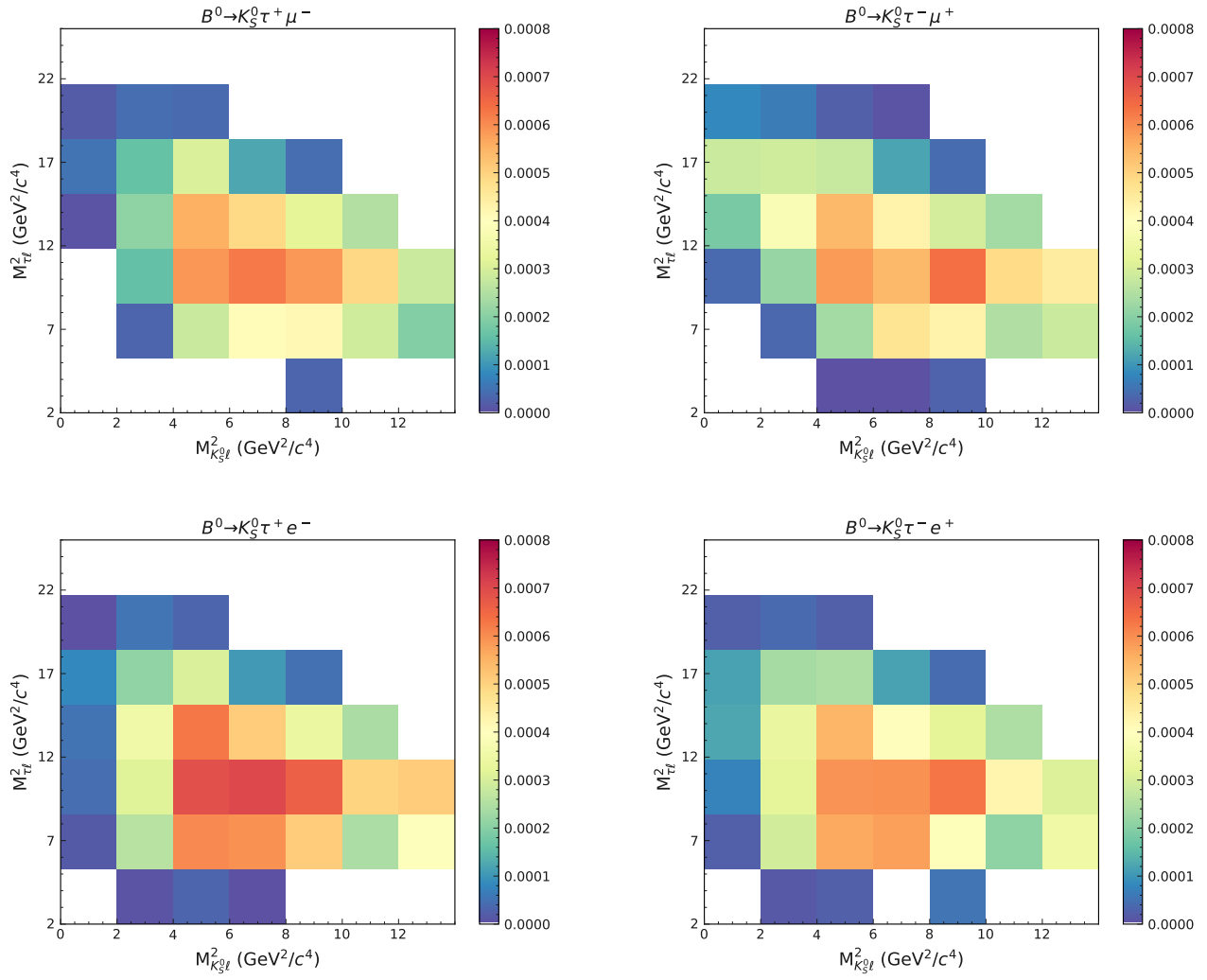


FIG. 1: Selection efficiency as a function of the kinematic variables $M^2(\tau\ell)$ and $M^2(K_S^0\ell)$.